

Structure and Spectra of Ferrous Dioxygen and Reduced Ferrous Dioxygen Model Cytochrome P450

Dan Harris,^{*,†} Gilda Loew,[†] and Lucy Waskell[‡]

Contribution from the Molecular Research Institute, 845 Page Mill Road, Palo Alto, California 94304, Department of Anesthesia and the Liver Center, University of California, San Francisco, California 94121, and the VA Medical Center, San Francisco, CA 94121

Received December 3, 1997. Revised Manuscript Received March 12, 1998

Abstract: The optimized geometries of the stable ferrous dioxygen and transient reduced ferrous dioxygen forms of a methylmercaptate porphine model of the cytochrome P450 heme system were calculated using nonlocal density functional theoretical (DFT) methods. The optimized geometry of the ferrous dioxygen form is in good agreement with the structure of a model compound of this species and the calculated diamagnetic singlet ground state is consistent with the reported lack of ESR spectrum of this species. The calculated ground state of the reduced ferrous dioxygen species is a low-spin (doublet) state, in agreement with the reported ESR signature of this species in P450cam. The dioxygen ligand in the reduced form is shown to preferentially bind to the heme iron in an asymmetric “end-on” geometry. The most pronounced structural effects of the reduction of the ferrous dioxygen species are the elongation of the Fe–O and Fe–S bonds. This bond lengthening is due to the addition of an electron into a molecular orbital of significant antibonding character in the S–Fe–O bonding upon reduction of the ferrous dioxygen species. The molecular electrostatic potential of the ferrous dioxygen and reduced ferrous dioxygen P450 intermediates both have pronounced minima near each of the bound dioxygen atoms, but with significantly lower minima in the reduced species. INDO/S/CI calculations of spectral and electronic properties were performed at the computed density functional geometries. The diamagnetic singlet ground state of the ferrous dioxygen and the doublet ground state of the reduced ferrous dioxygen species found with inclusion of configuration interaction are in agreement with the DFT results. The INDO/S/CI spectra of the ferrous dioxygen and reduced ferrous dioxygen species both have a split Soret band, due to mixing of the sulfur p orbitals with the porphyrin π orbitals modulated by the dioxygen ligands. Comparison of the computed spectra of these species with the reported experimental spectra show similar split-Soret signatures and spectral shifts compared to the ferric high-spin substrate bound state. The agreement between calculated and experimental spectra provides additional evidence that the species which are the origin of the observed spectra are indeed the ferrous dioxygen and reduced ferrous dioxygen P450 species.

Introduction

Cytochrome P450s, a ubiquitous class of enzymes with over 300 members, perform a variety of monooxygenation reactions including aliphatic and aromatic hydroxylations, epoxidations, and heteroatom oxidation. The preponderance of evidence suggests that these enzymes catalyze monooxygenation reactions by transfer of a single oxygen atom from a common active oxidative species, compound I, a ferryl oxygen (Fe=O) adduct of the heme unit. Formation of this common oxidative intermediate is believed to take place via a common mechanism for all P450 enzymes shown schematically in Figure 1. Substrate binds to the ferric resting form followed by an initial one-electron reduction to the substrate-bound ferrous species. Molecular oxygen then binds as a ligand to the heme iron, thus forming a ferrous dioxygen species, the last metastable intermediate. A second one-electron reduction of the ferrous dioxygen form follows and results in formation of the reduced ferrous dioxygen species. This species, with the addition of two protons, rapidly forms compound I and water. Compound I then oxidizes substrates by transfer of the active oxygen atom,

forming products and returning to the ferric resting state of the enzyme. All steps in the enzymatic cycle described after formation of the ferrous dioxygen species occur extremely rapidly making definitive characterization of the transient intermediates evoked in these steps very difficult. There have been no X-ray crystal structures reported for the ferrous dioxygen species, the reduced ferrous dioxygen species, or compound I for any of the P450 isozymes.

Of the three oxygen-containing intermediates in the P450 enzymatic cycle, most is known about the ferrous dioxygen species because it is stable enough to have been characterized by a number of spectroscopic methods. An EXAFS study of the ferrous dioxygen intermediate in P450cam^{1,2} as well as an X-ray structure of a model dioxygen P450 heme complex³ have been reported. In the crystal structure of this model compound, the oxygen is bound in an asymmetric “end-on” fashion to the heme iron. In addition to structural information, a number of

(1) Dawson, J. H.; Kau, L.-S.; Penner-Hahn, J. E.; Sono, M.; Eble, K. S.; Bruce, G. S.; Hager, L. P.; Hodgson, K. O. *J. Am. Chem. Soc.* **1986**, *108*, 8114.

(2) Dawson, J. H.; Sono, M. *Chem. Rev.* **1987**, *87*, 1255.

(3) Schappacher, M.; Ricard, L.; Fischer, J.; Weiss, R.; Bill, E.; Montiel-Montoya, R.; Winkler, H.; Trautwein, A. X. *Eur. J. Biochem.* **1987**, *168*, 419–430.

[†] Molecular Research Institute.

[‡] University of California, San Francisco, California 94121, and VA Medical Center, San Francisco.

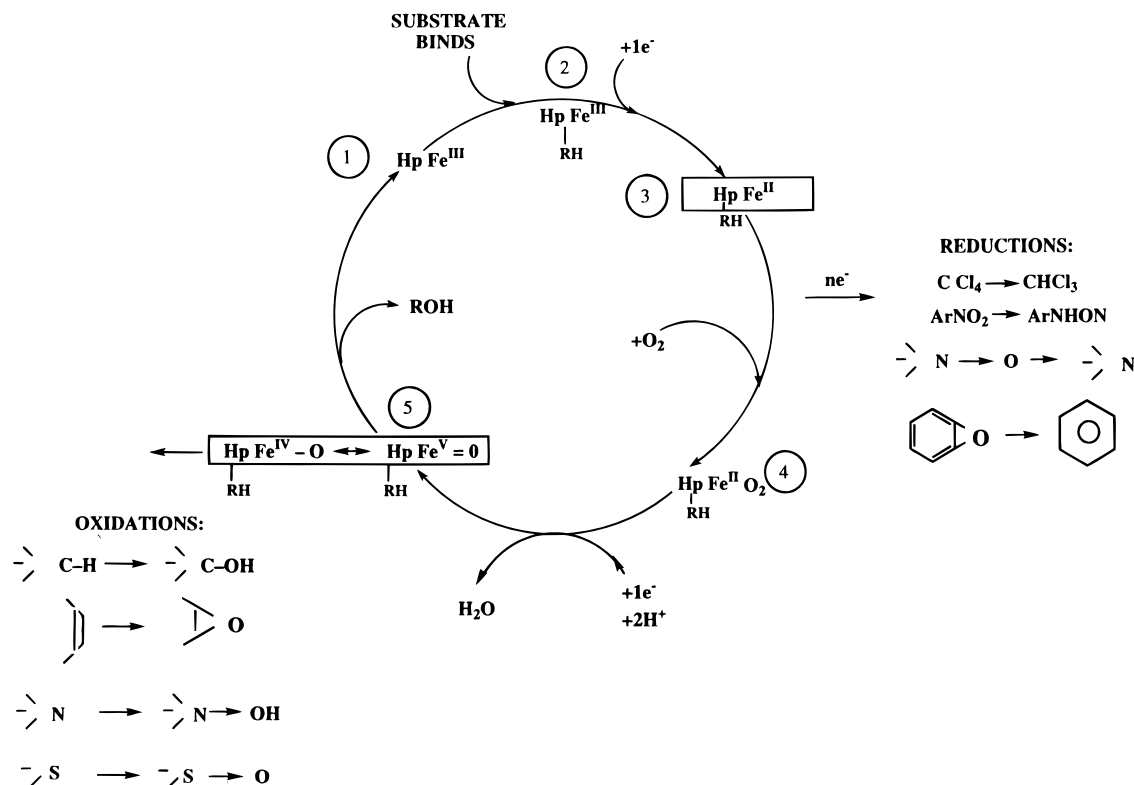


Figure 1. The proposed enzymatic cycle common to cytochrome P450s.

spectroscopic properties have been measured for both the ferrous dioxygen P450*cam* species and the ferrous dioxygen P450 heme model compound. The ferrous dioxygen P450*cam* species lacks an ESR signal^{4,5} and has had its Mossbauer^{6,7} and Q-band visible spectrum characterized.⁴ Resonance Raman studies, in conjunction with isotopic labeling, have associated the 1140 cm^{-1} band with the O–O stretching frequency of the bound dioxygen.⁸ The measured spectroscopic properties of the model compound include its vis–UV, ESR, and Mossbauer spectra.³ These are all similar to the ferrous dioxygen species of cytochrome P450*cam*.

Because of its transient nature, the effect of this second electron reduction on the geometry of the dioxygen ligand, and on the electronic structure and spin state of the reduced oxy ferrous species is unknown. The dioxygen ligand in this twice-reduced form, could remain in the end-on binding mode, or as suggested in the literature might correspond to a bridged, dioxygen-bound structure similar to that in five-coordinate ferric hemes⁹ and six-coordinate heme complexes of other transition metal ions.^{10,11} It has not been possible, however, to establish the preferred binding mode from experiment alone.

Two types of spectra, thought to originate from the reduced ferrous dioxygen P450*cam* species, have now been reported.

The ESR signature of the reduced ferrous dioxygen species in P450*cam*, generated by irradiation of the ferrous dioxygen P450*cam* species has been reported.⁴ More recently, a complete spectrum, including both the UV Soret and visible Q-band regions, of the putative reduced ferrous dioxygen species of P450*cam* has appeared.¹² Although plausible, neither the ESR nor the electronic spectra measurements reported provided independent definitive evidence that the species from which they originated is indeed the elusive twice-reduced ferrous dioxygen form. Nor can the geometry or mode of binding of the dioxygen species be deduced from these studies. The techniques of quantum chemistry are ideally suited to further probe the existence and the nature of the reduced ferrous dioxygen species. In the work reported here we have used the combined techniques of ab initio and semiempirical quantum chemistry to address these unresolved aspects of the enzymatic cycle common to all P450 enzymes.

Computation of optimized geometries, energies, and electronic structure of transition metal containing systems is known to require extensive electron correlation effects. DFT methods based on the seminal work of Hohenberg, Kohn, and Sham^{13,14} are promising alternatives to the traditional ab initio methods for characterizing these systems because they include electron correlation in the exchange–correlation functional and are not as computationally intensive as traditional correlated electron SCF methods such as multiconfigurational configuration interaction (MC–SCF–CI) methods. The use of nonlocal corrections has been demonstrated to improve the accuracy of transition metal–ligand and metal–metal bond distances,¹⁵ as well as the structure and thermochemistry of iron chlorides and

(4) Davydov, R.; Kappl, R.; Huttermann, J.; Peterson, J. A. *FEBS* **1991**, *295*, 113.

(5) Kobayashi, K.; Iwamoto, T.; Honda, K. *Biochem. Biophys. Res. Commun.* **1994**, *201*, 1348.

(6) Peterson, J. A.; Ishimura, Y.; Griffin, B. W. *Arch. Biochem. Biophys.* **1972**, *149*, 197.

(7) Sharrock, M.; Debrunner, P. G.; Schulz, C.; Lipscomb, J. D.; Marshall, V.; Gunsalus, I. C. *Biochim. Biophys. Acta* **1976**, *420*, 8.

(8) Bangcharoenpaupong, O.; Rizos, A. K.; Champion, P. M.; Jollie, D.; Sligar, S. G. *J. Biol. Chem.* **1986**, *261*, 8089.

(9) Burstyn, J. N.; Roe, J. A.; Miksztal, A. R.; Shaevitz, B. A.; Lang, G.; Valentine, J. S. *J. Am. Chem. Soc.* **1988**, *110*, 1382.

(10) Smith, T. D.; Podborow, J. R. *Coord. Chem. Rev.*, **1981**, *39*, 295.

(11) Tovrog, B. S.; Kitko, D. J.; Drago, R. S. *J. Am. Chem. Soc.* **1976**, *98*, 5144.

(12) Benson, D. E.; Suslick, K. S.; Sligar, S. G. *Biochemistry* **1997**, *36*, 5104.

(13) Hohenberg, P.; Kohn, W. *J. Phys. Rev. B* **1964**, *136*, 864.

(14) Kohn, W.; Sham, L. *J. Phys. Rev. A* **1965**, *140*, 1133.

(15) Fan, L.; Ziegler, T. *J. Chem. Phys.* **1991**, *95*, 7401.

their positive and negative ions.¹⁶ Nonlocal DFT has also been applied to a range of systems of biochemical interest including optimized geometries for a five-coordinate model of the ferryl heme complex,¹⁷ and iron sulfur clusters relevant to these centers in proteins.¹⁸ It has most recently been applied to the calculation of the properties of compound I in peroxidases at experimentally determined geometries¹⁹ and to the calculation of the equilibrium geometries and electronic structure of a number of five- and six-coordinate iron porphyrin complexes with CO, O₂, NO, and imidazole as ligands.²⁰ In other studies nonlocal DFT has also been shown to perform well for open-shell systems with unpaired spin density in a number of studies.²¹

While density functional theory was originally cast for the ground state,^{1,3} it is equally valid to apply it to the lowest excited states with different spin multiplicities and symmetries.²² DFT has been shown to provide an adequate prediction of the ground-state spin multiplicity of a number of diradicals as well the singlet–triplet energy gaps in a series of carbenes and nitrenium ions.²³ Our previous studies of the ground-state structure and vertical transition energies of ferric–hexaqua complexes indicated nonlocal DFT theory using BPW91 functionals were more accurate than DFT calculations using BLYP functionals or Möller–Plesset (MP2) results.²⁴ These results provide encouraging support for the use of the nonlocal DFT in this study to determine the optimized geometries and relative energies of the singlet and triplet states of the ferrous dioxygen P450 heme species and of the doublet and quartet states of the reduced ferrous dioxygen P450 heme species.

The INDO/S/ROHF/CI method has been shown to correctly calculate the ground state for a series of 23 model heme complexes with known high-, low-, and intermediate-spin ground states. In addition, this method accurately calculated their known Mossbauer and ESR hyperfine splitting parameters.²⁵ Even more extensive use and validation of the INDO/S/CI method has been made for calculation of electronic spectra^{26–30} as well as to predict changes in spectra as a function of electronic spin state.³¹ Given reasonable experimental or calculated geometries, the semiempirical INDO/S/CI method

has been shown in these studies to be capable of calculation of spectra and electronic properties of transition metal complexes. As a consequence of the use of only single excitations to calculate spectra, calculated transition energies may differ from experiment by 20–50 nm depending on the spectral region. However, spectral shifts resulting from changes in ligand, spin state, or oxidation state of the heme are accurately predicted. The main use to be made of the INDO/S/ROHF/CI method is to calculate and compare the spectra of the ferrous dioxygen and reduced ferrous dioxygen species using the DFT-optimized geometries of these two species.

In these studies, the nonlocal density function method has been used to obtain optimized geometries, ground-state spin distributions, and electronic structure of the ferrous dioxygen and reduced ferrous dioxygen P450 heme complexes. The ferrous dioxygen species was included in these studies in order to continue to assess the reliability of the nonlocal DFT by comparison of the calculated properties of this well characterized species with experiment. After successful validation, the same methods and procedures were used to further probe the existence and the nature of the more elusive reduced ferrous dioxygen species.

An INDO/S/ROHF/CI restricted open-shell Hartree–Fock configuration interaction method has then been used to calculate the electronic spectra of these two species at DFT optimized geometries. The calculated spectra of these intermediates were compared with the recently published spectra of these putative species. These comparisons should help to further identify the species that are the origin of these observed spectra and provide assignment of the electronic excitations comprising the observed absorption bands.

Methods

Model Used and Choice of Initial Geometries. The model of the P450 heme site used in all DFT calculations is an iron–porphyrin complex with no porphyrin substituents and a methyl mercaptide (SCH₃[−]) axial ligand for the heme iron. The initial geometry chosen for the ferrous dioxygen species was based on the Weiss model compound structure.³ Thus, an initial bent end-on dioxygen geometry was used for this species in which only one oxygen atom binds directly to the heme iron. The initial Fe–S, Fe–O, Fe–N, and O–O distances used were 2.3, 1.8, 2.0, and 1.3 Å, respectively, and an initial Fe–O1–O2 bond angle of 120° was used.

For the initial structure of the reduced ferrous dioxygen species, the optimized geometry for the end-on structure of the ferrous dioxygen species was used. In addition to this initial end-on geometry, a second initial geometry, with the dioxygen bound to the heme iron in a symmetric “side on”, bridged mode with both oxygen atoms as ligands was constructed for the reduced ferrous dioxygen species. In this initial configuration the two equal initial iron–oxygen distances were 1.84 Å. This initial geometry was generated using the UNICHEM 4 interface.³²

Density Functional DFT Calculations. Density functional calculations were performed using DGauss version 4.0 in conjunction with the UNICHEM interface.³² All DFT calculations were performed using Becke’s 1988 functional, which includes the Slater exchange along corrections involving the gradient in the density (nonlocal corrections).³³ Two types of gradient corrected correlation functions were used, either the Perdew–Wang-’91 (BPW91)³⁴ or the Lee–Yang–Parr (BLYP)

(16) Bach, R. D.; Schobe, D. S.; Schlegel, H. B. *J. Phys. Chem.* **1996**, *100*, 8770.

(17) Ghosh, A.; Almlof, J.; Que, L., Jr. *J. Am. Chem. Soc.* **1993**, *98*, 5576.

(18) Mouesca, J.-M.; Chen, J. L.; Noodleman, L.; Bashford, D.; Case, D. A. *J. Am. Chem. Soc.* **1994**, *116*, 11898.

(19) Kuramochi, H.; Noodleman, L.; Case, D. A. *J. Am. Chem. Soc.* **1997**, *119*, 11442–11451.

(20) Rovira, C.; Kunc, K.; Hutter, J.; Ballone, P.; Parrinello, M. *J. Phys. Chem.* **1997**, *101*, 8914–8925.

(21) (a) Cramer, C. W.; Dulles, F. J.; Falvey, D. E. *J. Am. Chem. Soc.* **1994**, *116*, 9797. (b) Baker, J.; Scheiner, A.; Anzelm, J. *Chem. Phys. Lett.* **1993**, *216*, 380–388. (c) Murry, C. W.; Handy, N. C.; Amos, R. D. *J. Chem. Phys.* **1993**, *98*, 7145.

(22) Gunnarsson, O.; Lundqvist, B. I. *Phys. Rev. B* **1976**, *13*, 4274.

(23) Lim, M. H.; Worthington, S. E.; Dulles, F. J.; Cramer, C. J. In *Density Functional Methods in Chemistry*; Laird, B. B., Ziegler, T., Ross, R., Eds.; ACS Symposium Series; American Chemical Society: Washington, DC, 1996.

(24) Harris, D.; Loew, G. H.; Komornicki, A. *J. Phys. Chem.* **1997**, *101*, 3959.

(25) Axe, F. R.; Flowers, C.; Loew, G. H.; Waleh, A. J. *J. Am. Chem. Soc.* **1989**, *111*, 733.

(26) Herman, Z. S.; Loew, G. H. *J. Am. Chem. Soc.* **1980**, *102*, 1815.

(27) Rohmer, M. M.; Loew, G. H. *Int. J. Quantum Chem.* **1979**, *6*, 93.

(28) Loew, G. H.; Rohmer, M. M. *J. Am. Chem. Soc.* **1980**, *102*, 3655.

(29) Loew, G. H.; Herman, Z. S.; Rohmer, M. M.; Goldblum, A.; Pudzianowski, A. *Structure, Spectra and Function of Model Cytochrome P450*. In *Quantum Chemistry in Biomedical Sciences*; Weinstein, H., Green, J. P., Eds.; The New York Academy of Sciences: New York, 1981; Vol. 367, p 192.

(30) Harris, D. L.; Loew, G. H. *J. Am. Chem. Soc.* **1996**, *118*, 10588.

(31) Harris, D. L.; Loew, G. H., *J. Am. Chem. Soc.* **1993**, *115*, 5799.

(32) Dgauss 4.0/Unichem Oxford Molecular, Beaverton, OR.

(33) Becke, A. D. *Phys. Rev. A* **1988**, *38*, 3098.

gradient-corrected correlation functionals,³⁵ and the results from each were compared.

A double- ζ valence polarization basis (DZVP) set was used in all calculations. These include diffuse d functions on all atoms except hydrogen. In selected calculations using the BLYP functional, an additional sp shell, with an exponent of 0.0405, was added to the standard DZVP sulfur description since this atom had significant anionic character. The atomic basis sets in DGauss employed atomic centered Gaussian basis functions optimized for use with DFT.^{36,37}

This program employs an additional auxiliary approximation in the use of the fitting basis,³⁸ to express the charge density in a series expansion in Gaussian basis functions. The energy expression, employing this fitting basis, may be computed in order N^3 in contrast to the exact energy expression which scales as N^4 . Assessment of the use of this approximation in reproducing the results for small compounds containing iron previously examined by Bauchlicher using couple cluster methods were found to be well reproduced.

In all calculations, a fine density grid was chosen ($\sim 10^7$ 844 grid points). All the SCF iterations were converged to 2×10^{-6} in the density matrix and 2×10^{-8} in the energy. All optimizations converged within the chosen criterion of 0.0008 hartrees/Å. All calculations were made using 2-CPU's of a J90 provided by Oxford Molecular, Beaverton, OR.

Optimized geometries were obtained for both singlet and triplet states of the ferrous dioxygen species and for doublet and quartet states of the reduced ferrous dioxygen species using the unrestricted density functional code embodied in DGauss.³² The structure and electronic description of the ground state was determined as the lower energy of the two spin state alternatives for each species. Spectra of these porphine models of the P450 oxy intermediates, at their optimized DFT geometries, were then calculated using an INDO/S/CI procedure described below.

Generation of a Protoporphyrin IX Heme Model for Each Species. In addition to calculations of spectra of ferrous and reduced ferrous dioxygen bound porphine models of the corresponding P450 intermediates at DFT optimized geometries, the spectra of the full protoporphyrin IX heme model of each P450 species were calculated. The geometry of these heme models was generated using a combination of the results obtained from the nonlocal DFT-optimized geometries for the unsubstituted porphine and the existing parameters in the AMBER 4.1³⁹ suite of programs for the added substituents. The steps used in this procedures were (1) the porphine structural parameters (bond lengths, bond angles, and torsion angles) determined from DFT geometry optimizations of the ferrous and reduced ferrous dioxygen porphine species were introduced into the AMBER 4.1 (Oxford Molecular, Beaverton, OR) parameter database, (2) the substituents corresponding to protoporphyrin IX were added to this porphine core using and parameters for these substituents developed previously for the reduced ferrous dioxygen heme form,³⁰ (3) the resulting full protoporphyrin-IX models of the ferrous dioxygen and reduced

ferrous dioxygen intermediates were then energy-minimized using the SANDER module of AMBER 4.1. These were the minimized structures that were employed in the INDO/S/ROHF/CI calculations. The calculated spectrum of the high spin, substrate bound ferric P450 heme species shown here for comparison also employed a full protoporphyrin-IX model prepared in a comparable fashion as input for INDO/S/ROHF/CI, as previously reported.³¹

INDO/S/ROHF/CI Spectra and Calculated Ground-State Properties. These calculations were performed using an INDO/S restricted open-shell Hartree–Fock configuration interaction (INDO/S–ROHF/CI) method.^{40,41} Using the DFT-optimized ground-state geometries for both the ferrous dioxygen and reduced ferrous dioxygen porphine species, INDO/S calculations were made first without and then with configuration interaction. The configurations included were a limited set of double excitations, expected to couple most strongly with the initial reference configuration. The calculations with and without CI were compared to ascertain the importance of electron correlation, within the context of the INDO/S method, in determining the spin multiplicity of the ground state of the oxy intermediates.

The spin state species determined to be the ground state for each species was used as the reference for configuration interaction (CI) calculations of the electronic spectra for that entity. In cases where electron correlation was determined to be important and a single configuration was dominant, this dominant configuration was used as the reference to calculate spectra of the oxy intermediate species.

The spectra were calculated from a single excitations CI employing the Tamm–Dancoff approximation, in which each excited state is approximated as a linear combination of single excitations, i.e., the energy of the system with a promoted electron is approximated by the energy for such a promotion with orbital energies given by the solution for the ground state of the molecule. Such an approximation tends to overestimate the wavelength corresponding to the transition by 20–50 nm depending on the spectral region. This level of calculation is, however, adequate for the accurate prediction of spectral shifts resulting from changes in ligand, spin state, or oxidation state of the heme. The main use to be made of the INDO/S/ROHF/CI method is to calculate and compare the spectra of the ferrous dioxygen and reduced ferrous dioxygen species using the DFT-optimized geometries of these two species.

The excitations in the CI were chosen in accord with the Rumer procedure in which the spin multiplicity of the CI states were taken to be the same as the reference state. The excitation space explored in the CI for all three species considered in this study included the filled $1e_g$, $2e_g$, $3e_g$, $1a_{1u}$, $2a_{2u}$, $3a_{2u}$ porphine/porphyrin π orbitals into the unfilled $4e_g(\pi^*)$ and $2b_{1u}(\pi^*)$ and iron d orbitals. The excitation space also included all orbitals containing S and O character admixed with orbitals of porphine/porphyrin π and π^* character. Wherever possible, the symmetry labels used for the orbitals on the heme/porphine are idealized for $D4h$ symmetry analogous to the porphine core of the porphyrin without substituents, although these complexes deviate slightly from this ideal symmetry. In selected cases where ligand perturbation of the $D4h$ symmetry is significant, symmetry assignments have been used in the appropriate symmetry subgroup, which is applicable due to the perturbation.

The roots of the CI matrix were used to calculate the frequencies of the electronic transitions. The electric dipole

(34) Perdew, J. P.; Wang, Y. *Phys. Rev. B* **1992**, *45*, 13244.

(35) Lee, C.; Yang, W.; Parr, R. G. *Phys. Rev. B* **1988**, *37*, 785.

(36) Godbout, N.; Salahub, D. R.; Andzelm, J.; Wimmer, E. *Can. J. Chem.* **1992**, *70*, 560.

(37) Sosa, C.; Andzelm, J.; Elkin, B. C.; Wimmer, E.; Dobbs K. D.; Dixon, D. A. *J. Phys. Chem.* **1992**, *96*, 6630.

(38) (a) Dunlap, B. I.; Connolly, J. W. D.; Sabin, J. R. *J. Chem. Phys.* **1979**, *71*, 3396. (b) Dunlap, B. I.; Connolly, J. W. D.; Sabin, J. R. *J. Chem. Phys.* **1979**, *71*, 4993.

(39) Cornell, W. D.; Cieplak, P.; Bayly, C. I.; Gould, I. R.; Merz, K. M., Jr.; Fefuson, D. M.; Spellmeyer, D. D.; Fox, T.; Caldwell, J. W.; Kollman, P. A. *J. Am. Chem. Soc.* **1995**, *117*, 5179–5197.

(40) Bacon, A. D.; Zerner, M. C. *Theor. Chim. Acta* **1979**, *53*, 21.

(41) Edwards, W. D.; Zerner, M. C. *Theor. Chim. Acta* **1987**, *72*, 347.

matrix elements were used to calculate oscillator strengths for each transition corresponding to the intensity of the transition. Together these quantities, a list of frequencies, oscillator strengths, and contributions to the intensity from the *x*, *y*, and *z* components of the transition moment comprise the spectrum of each species. These results can therefore be presented as "delta function" spectral lines (stick figures) in a frequency/intensity plot in which the position on the abscissa axis indicates the frequency and the height represents its intensity, as well as in tabular form.

In addition, a simple model spectrum was generated from the sums of uniform width Gaussians convoluted with the "delta function" spectral lines. In this procedure, a Gaussian with a uniform line width of 1500 cm⁻¹ was convoluted with each spectral line and the results summed to generate a total spectral contour. The amplitude at the Gaussian center was determined by the oscillator strength of that underlying spectral line. The primary data are the spectral line intensities and frequencies, but the convoluted band contours are generated in order to make the most consistent comparisons with the experimental spectra.

Assignment of each of these spectral lines in terms of the type of excitations contributing to them was also made. These spectral line assignments are expressed in terms of % contribution of specific molecular orbital excitations. There is no case where a single excitation is responsible for a given spectral line. Each of the calculated frequencies has intensity contributions from many fundamental excitations.

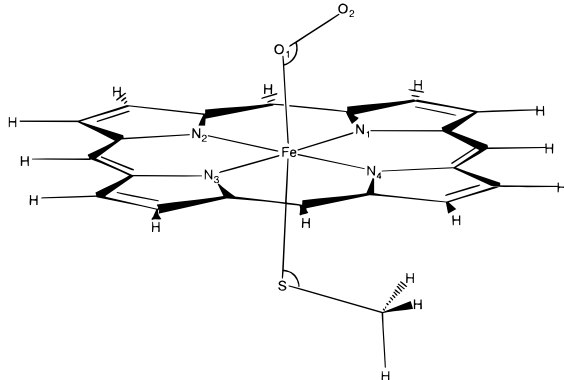
Results and Discussion

Optimized Geometries. Table 1 gives the DFT-optimized geometries for ground states of the ferrous dioxygen and reduced ferrous dioxygen P450 heme complex using both the BLYP and BPW91 functionals. Also presented in Table 1, for comparison are the experimental values of the geometric quantities found in the X-ray structure of a model ferrous dioxygen P450 heme³ and the very similar values found in EXAFS measurements of this species in intact P450cam and chloroperoxidase heme proteins.² As shown in Table 1, the ground-state geometries for the ferrous dioxygen P450 heme complex calculated with either BLYP and BPW91 functionals are in good agreement with the experimentally determined geometric quantities. The exception is the O–O bond length. The calculated distance is more reliable for this quantity because the free rotation around the Fe–O bond prevented its accurate determination in the X-ray structure of the model compound.

The agreement between calculated and observed geometries for the ferrous dioxygen P450 heme complex provides evidence for the reliability of the nonlocal DFT methods to obtain optimized geometries for the reduced ferrous dioxygen P450 species for which there is no experimental structural information. In the absence of such information, two postulated structures were considered in this study, both of which are defined in Figure 2. The first was the asymmetric end-on geometry similar to the ferrous dioxygen species shown in panel A of Figure 2. The other was a symmetric side-on bridged structure, shown in panel B of Figure 2. This geometry was postulated on the basis of structural evidence for such symmetric dioxygen coordination in five-coordinate model ferric heme complexes⁹ and in heme complexes of transition metals other than iron.^{42,43}

Initial geometries for both the end-on and bridged geometries were constructed, and energy optimized structures for each were

Table 1. Optimized Geometries^a of Ferrous Dioxygen and Reduced Ferrous Dioxygen Porphine Model P450 Species Calculated Using Nonlocal DFT with the BLYP and BPW91 Functionals



geometric quantity	ferrous dioxygen species		reduced
	experiment	BPW91 (BLYP)	ferrous dioxygen BPW91 (BLYP)
Fe–O1	1.82 (1.78) ^c	1.82 (1.83)	1.95 (1.95)
O1–O2	1.14 ^b	1.31 (1.32)	1.33 (1.35)
Fe–N1	1.98 (2.0) ^c	2.01 (2.03)	2.01 (2.02)
Fe–N2	1.99	2.01 (2.03)	2.01 (2.02)
Fe–N3	2.01	2.04 (2.06)	2.03 (2.05)
Fe–N4	1.99	2.04 (2.06)	2.03 (2.05)
Fe–S	2.37 (2.37) ^c	2.32 (2.37)	2.46 (2.60)
C2–S	1.72	1.84 (1.85)	1.85 (1.86)
∠Fe–O1–O2	128	122 (122)	120 (119)
∠S–Fe–O1	177	173 (173)	175 (176)
∠C–S1–Fe		110 (109)	109 (108)
∠N4–Fe–O1–O2	23–45	45 (45)	45 (45)
∠C–S–Fe–N4		45 (45)	45 (45)

^a Distances in angstroms and angles in degrees. ^b Position of O₂ disordered in model compound crystal structure resulting in O1–O2 inaccuracy. ^c Experimental values from ref 2; values in parentheses from ref 3.

obtained, indicating that the reduced ferrous dioxygen species is stable, i.e., a bound nondissociative species albeit extremely reactive, and in this sense, a transient species.

The optimized reduced oxy ferrous species with a symmetric bridged O₂ geometry, shown in Figure 2, panel B, had a much higher energy, 28 kcal/mol above the alternative form with an asymmetric end-on O₂ binding geometry shown in panel A of Figure 2. The high relative energy of the complex with the symmetric bridged O₂ binding mode indicates it not a viable candidate for the ground-state structure of this transient intermediate.

As seen in Table 1, the optimized geometry of the reduced ferrous dioxygen species in the preferred asymmetric end-on O₂ binding geometry is similar to that found for the ferrous dioxygen species. The primary effect of reduction of the ferrous dioxygen species is elongation of the Fe–S and Fe–O bonds with the magnitude of the Fe–S bond lengthening somewhat greater using the BLYP functional than using the BPW91 functional. While no structural information is available to critically assess these two different Fe–S bond lengths, BPW91 functionals generally perform better than BLYP functionals in describing the electron density in the outer regions of atoms and molecules.⁴⁴ Consequently, the DFT-optimized geometries obtained using the BPW91 functionals were chosen for computation of the spectra in the remainder of the study.

Examination of the filled and occupied orbitals of the ferrous dioxygen and reduced ferrous dioxygen species reveal the origin

(42) Smith, T. D.; Podborow, J. R. *Coord. Chem. Rev.*, **1981**, 39, 295.
 (43) Tovrog, B. S.; Kitko, D. J.; Drago, R. S. *J. Am. Chem. Soc.* **1976**, 98, 5144.

(44) Laidig, K. E. *Chem. Phys. Lett.* **1994**, 225, 285.

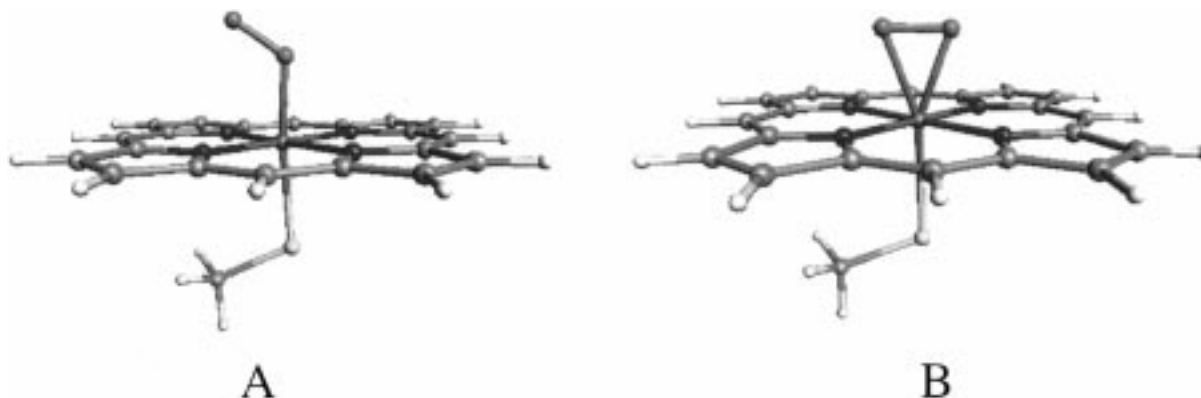


Figure 2. The optimized structures of both the (A) asymmetric “end-on” and (B) symmetric, side-on, “bridged” form of the porphine models of the P450 reduced ferrous dioxygen species obtained using the DFT method. The energy of symmetric side on form is 28 kcal/mol higher than the asymmetric “end-on” reduced ferrous dioxygen with only one oxygen atom as a ligand to the heme iron, as shown in Table 1. The methyl mercapto group replacement of the P450 cysteine ligand and the bound dioxygen are bound to the iron on opposite sides of the porphine. Atom types are color coded: carbons (green), hydrogens (white), nitrogens (blue), sulfur (yellow), oxygens (light red), and iron (dark red).



Figure 3. The lowest unoccupied molecular orbital of the ferrous dioxygen porphine P450 species to which an electron is added upon reduction. The red and blue colors indicate the sign of the wave function of this molecular orbital and illustrate that it has antibonding S–Fe–O character.

of the Fe–O and Fe–S bond lengthening. Upon reduction of the ferrous dioxygen species, the added electron occupies a molecular orbital of significant antibonding character on the S–Fe–O centers, shown in Figure 3, that was previously empty. It is this added electron occupancy that leads to the pronounced Fe–O and Fe–S bond elongation upon reduction. However, this second electron reduction does not significantly weaken the O–O bond (cf. Table 1) as reflected in the Mayer bond orders. Thus, facile O–O bond cleavage to form the oxyferryl compound I species, requires the proton-assisted cleavage of this bond as supported by experimental kinetic isotope effects.⁴⁵

Characterization of Ground and Excited States of Different Spin Multiplicity. Table 2 gives relative energies of the optimized ferrous dioxygen singlet and triplet P450 species and of the optimized reduced ferrous dioxygen doublet and quartet states in the favored end-on geometry from the nonlocal DFT calculations. These results indicate that the diamagnetic singlet ferrous dioxygen species is the ground state with very low lying triplet states of comparable energy using either the BPW91 or BLYP nonlocal functionals, in agreement with the lack of an ESR signal from this species.^{4,5} In contrast to the ferrous dioxygen species, with a very low lying state of higher

Table 2. Energies (in kcal/mol) of Spin States of Ferrous Dioxygen and Reduced Ferrous Dioxygen Porphine P450 Species Calculated Using Nonlocal DFT and INDO/S (both with and without configuration interaction)

method	ferrous dioxygen		reduced ferrous dioxygen	
	singlet ($S = 0$)	triplet ($S = 1$)	doublet ($S = 1/2$)	quartet ($S = 3/2$)
BLYP	0.0	0.8	0.0	11.3
BPW91	0.0	1.1	0.0	10.0
INDO/S	43.1	0.0	1.9	0.0
INDO/S/CI	0.5	0.0	0.0	1.6

multiplicity, in the reduced system, using both the BLYP and BPW91 functionals, there is a larger energy difference of 10–11 kcal/mol for the quartet state. Davydov and Peterson have measured an ESR spectrum of the reduced ferrous dioxygen species, generated by irradiation of the ferrous dioxygen species in cytochrome P450cam, consistent with a low-spin doublet state,⁴ thus providing experimental validation of the finding of a doublet ground state for this species from the DFT calculations.

In addition to determining that the consistency of the spin state ordering from the nonlocal DFT results for the two dioxygen species with experiment, it was important also to determine if spin state ordering obtained from use of the INDO/S/ROHF/CI method at the BPW91 density functional geometries gave similar results, since this method is the one to be used to calculate spectra of these species. As shown in Table 2, spin-state ordering for the ferrous and reduced ferrous dioxygen porphine P450 species determined from INDO/S calculations at the BPW91 density functional geometries are in agreement with the DFT and experiment results only when configuration interaction is included in these calculations. For the ferrous dioxygen species a singlet state energy essentially degenerate, i.e., within 0.5 kcal/mol with the triplet state results. For the reduced ferrous dioxygen species a doublet state is the ground state. Given the *semiempirical* and minimal basis set nature of this INDO/S/ROHF/CI method, this level of agreement with experiment and the density functional calculations is surprisingly good.

Table 3 indicates the excess spin densities on the iron, oxygen, sulfur, and porphine atoms for the reduced ferrous dioxygen species from both the density functional and INDO/S/ROHF/CI results. The spin distributions obtained for this species from both methods is found to be comparable, justifying the calculation of INDO/S/ROHF/CI spectra at the density functional porphine geometries. Both of these methods indicate that the

(45) Aikens, J.; Sliagar, S. *J. Am. Chem. Soc.*, **1994** *116*, 1143.

Table 3. Calculated Excess Spin Densities ($\rho^\uparrow - \rho^\downarrow$) of the Reduced Ferrous Dioxygen P450 Species

spin population on	INDO/S		BPW91	
	oxy-doublet	quartet	oxy-doublet	quartet
Fe	0.03	0.99	-0.22	0.60
O1 ^a	0.24	0.31	0.42	0.61
O2 ^a	0.73	0.68	0.51	0.68
S	0.0	0.0	-0.02	0.20
porphine π	0.0	1.02	+0.32	0.91

^a O1 is the proximal oxygen and O2 the distal oxygen.

Table 4. Calculated INDO/S Mossbauer Quadrupole Splitting (ΔE_Q) Parameters for Ferrous and Reduced Ferrous Dioxygen Porphine P450 Species

species	ΔE_Q (mm/s)
Ferrous Dioxygen Species	
singlet	2.34 (2.04, ^a 2.15 ^b)
triplet	3.91
Reduced Ferrous Dioxygen Species	
oxy-doublet	0.20
quartet	1.97

^a Experiment: Weiss model compound ref 3. ^b Experiment: P450cam ref 6.

ground state is an oxy doublet, with the preponderance of the unpaired spin density on the two oxygen atoms of the dioxygen ligand. The quartet state, calculated to be 10–11 kcal/mol higher than the ground-state doublet is seen to have an excess spin density more delocalized than the doublet case, distributed over the Fe, S, oxygen, and porphine atoms.

The density functional and INDO/S/ROHF/CI results indicate that the inclusion of electron correlation effects are crucial to proper prediction of the spin-state energy ordering of the dioxygen intermediates of the cytochrome P450 enzymes. Nevertheless, the INDO/S/ROHF/CI results indicate that a single configuration is dominant and is an adequate description of the electronic structure of each of these species. In the ferrous

dioxygen species, the spin-paired singlet reference configuration was the dominant configuration in the CI expansion (90%) consistent with the DFT results. In the reduced ferrous dioxygen P450 species, there is also only one significant reference configuration, a doublet, with a contribution 100 times larger than the contribution of any other state in the CI for this species. These dominant configurations were hence used as the reference configuration of the ground state for calculation of the spectra of these species discussed below.

Quadrupole Splitting (ΔE_Q) in Mossbauer Resonance Spectra. Table 4 shows the calculated Mossbauer quadrupole splittings (ΔE_Q) for the high and low spin states of each of the dioxygen porphine species. These results dramatically indicate the sensitivity of this quantity to the electronic configuration, oxidation state, and chemical bonding of the iron center. Experimental Mossbauer results for the ferrous dioxygen species of P450cam^{6,7} and the Weiss model compound³ have a ΔE_Q of 2.1 mm/s in good agreement with the calculated value of 2.34 mm/s for the singlet ground state of the ferrous dioxygen P450 model. The disparity of the experimental and calculated value of 3.91 mm/s for the triplet state provides further evidence for the validity of the singlet ground state. Calculated ΔE_Q values for the lowest energy doublet and quartet states of the reduced ferrous dioxygen species cannot be compared with experiment. However, the ground-state doublet value of 0.23 mm/s is the value predicted to correspond to experimental observation. This prediction can be used to further confirm the existence of such a species when and if it is trapped either in mutant, wt or model cytochrome P450.

Molecular Electrostatic Potentials of the Two Dioxygen P450 Heme Species. The DFT results obtained have clearly indicated that the second electron reduction alone is not sufficient to account for facile formation of compound I by cleavage of the O–O bond leading to the oxyferryl species. It is widely accepted that donation of two protons to the distal oxygen atom of the reduced ferrous dioxygen species are the

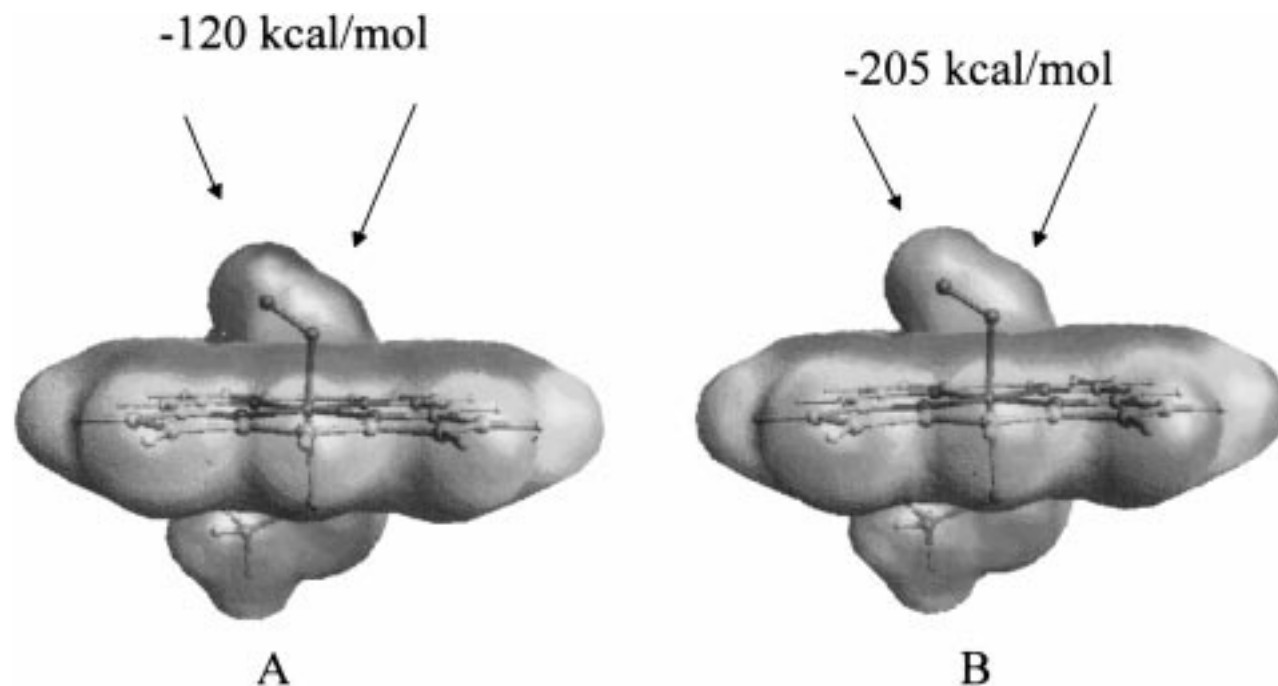


Figure 4. The computed molecular electrostatic potential (MEP) mapped on Connolly surface for (A) the ferrous dioxygen porphine P450 species from the DFT (BPW91) ground-state singlet wave function [MEP from blue (-120 kcal/mol) to red (-20 kcal/mol)] and (B) the reduced ferrous dioxygen porphine P450 species from the DFT (BPW91) ground state doublet wave function [MEP from blue (-205 kcal/mol) to red (-80 kcal/mol)].

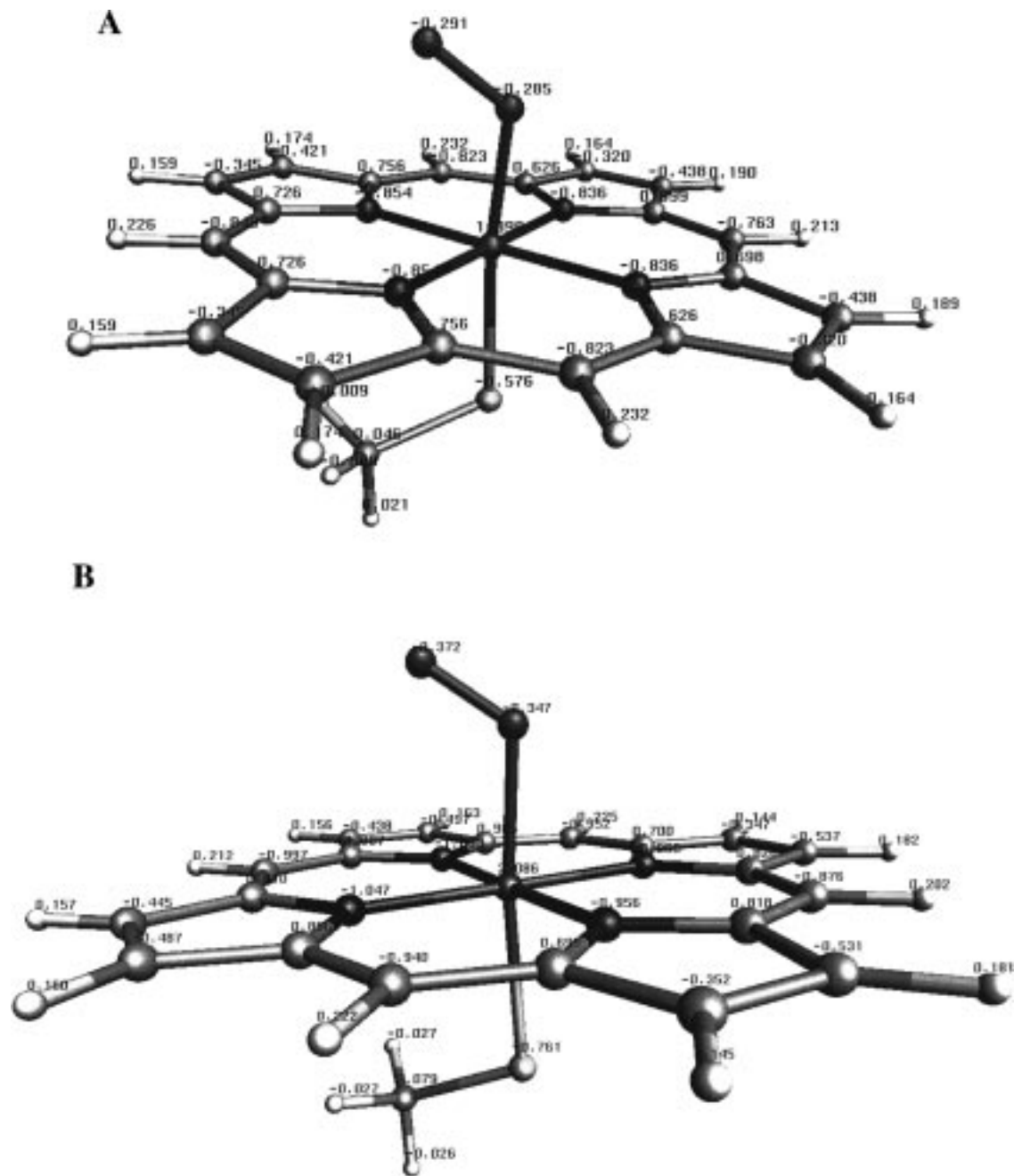


Figure 5. The MEPS derived charges at atom centers for (A) the ferrous dioxygen porphine P450 species and (B) the reduced ferrous dioxygen porphine P450 species.

next essential steps in facile O—O bond cleavage and compound I formation. The main experimental evidence for this inference is the known requirement of two protons and formation of water as well as compound I.⁴⁵ In addition, recent molecular dynamics studies of the reduced dioxygen bound species in wt P450eryF indicated two hydrogen bonds to the distal oxygen were present during most of the simulation indicating a coordination likely to facilitate diprotonation.³⁰

To continue to probe the plausibility of the proton-assisted mechanism of compound I formation, molecular electrostatic potentials (MEPs) and net atomic charges were computed for both the ferrous dioxygen and reduced ferrous dioxygen species. The minima in these MEPS correspond to the region of lowest energy for a positively charged species such as a proton or a hydrogen bonding hydrogen attached to a heteroatom.

In Figure 4, panel A shows the molecular electrostatic potential surface of the ferrous dioxygen porphine P450 species,

while panel B illustrates the MEPS surface for the reduced ferrous dioxygen porphine P450 species. The calculated MEPS were determined from the ground-state wave function computed using DFT(BPW91) for each species. Inspection of the two panels in Figure 4 shows that the region near the two oxygen atoms of both the ferrous and reduced ferrous dioxygen species have the most favorable sites for interaction with a species or functional group of electropositive character. However, the addition of an electron to the ferrous dioxygen species results in a significant increase in the depth of the minima near the dioxygen atoms in the reduced ferrous dioxygen species. The minima near the dioxygen atoms are -120 kcal for the ferrous dioxygen species and -205 kcal/mol for the reduced ferrous dioxygen species. Clearly the reduced ferrous dioxygen species will rapidly hydrogen bond to any species present in the binding site cavity which may serve as a hydrogen-bond donor. However, while the MEPS surface indicates about equal

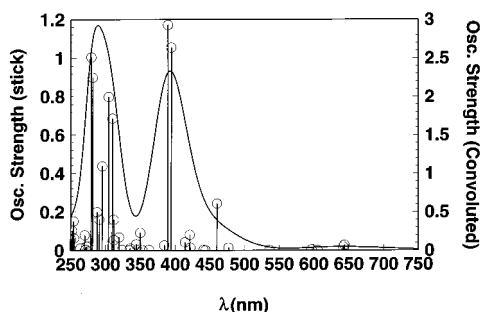


Figure 6. INDO/S/CI calculated spectrum of the ferrous dioxygen porphine model P450 species at the BPW91-optimized geometry.

likelihood for the approach of potential proton/hydrogen bond donors to either the proximal or distal oxygen, it does not give an indication of the relative propensity of the distal vs proximal oxygen sites toward proton addition, which requires the calculation of proton affinities.

Panels A and B of Figure 5 show the net atomic charges on each atom of the ferrous dioxygen and reduced ferrous dioxygen porphine P450 species obtained by fitting the calculated molecular electrostatic potential shown in Figure 4A,B. As seen in these figures, very similar negative charge on the distal than the proximal oxygen ligand are obtained consistent with the equivalent electrostatic potentials found near these two oxygen atoms. Upon one-electron reduction, the negative charge on each of the oxygen atoms increases. However, the increased

charge density on the oxygen atoms accounts for only a fraction of the electron density added with most of the additional electron density delocalized throughout the remainder of the system.

Electronic Spectra of the Two Dioxygen P450 Species.

Two distinct sets of spectra of the ferrous and reduced ferrous dioxygen species were calculated. One set was of the unsubstituted porphine models of each species calculated at the DFT-optimized geometries. The other set was with the methyl, vinyl, and propionate substituents on the porphine ring corresponding to protoporphyrin IX models of each species using the porphine geometric information as described in the methods. The spectral calculations of the unsubstituted porphyrin models allow more straightforward assignment of excitations contributing to the calculated spectra. They also clearly indicate the nature of the effects of the reduction of the ferrous dioxygen intermediate. The calculated spectra of the protoporphyrin IX models of the two dioxygen intermediates make the closest possible linkage with the form, giving rise to the experimental spectra of the actual P450 enzymes.

Figure 6 shows the spectrum of the ferrous dioxygen porphine P450 species calculated from single excitations using the INDO/S/CI method. Each of the calculated excitation lines in the spectrum is shown in Figure 6 as a vertical line. The Gaussian profile also shown in this figure is the Gaussian convoluted sum of these excitations, shown to make more facile qualitative comparison with reported experiment. The spectrum has a marked split-Soret signature.

Table 5. Assignment of Major Electron Excitations Comprising the Calculated Spectral Frequencies in the Soret (B,B') Region of the Spectrum of the Ferrous Dioxygen Porphine Model P450 Species Computed from a Singlet Ground-State Reference Configuration Using INDO/S CI at the DFT Optimized Geometry

λ (nm)	Osc. Str.	character, %	transition character	band character
280	1.00	13	$A''(\text{Cs})(\pi) \rightarrow 4e_g(\pi^*)$	
		62	$A'(\text{Cs})(\pi) + \text{Fe-O-S}(\sigma, \pi) \rightarrow 4e_g(\pi^*)$	
282	0.89	29	$A''(\text{Cs})(\pi) \rightarrow 4e_g(\pi^*)$	
		26	$A'(\text{Cs})(\pi) + \text{Fe-O-S}(\sigma, \pi) \rightarrow 4e_g(\pi^*)$	
288	0.19	12	$3e_g(\pi)/\text{Fe-O-S}(\sigma) \rightarrow b_{2u}(\pi^*)$	
		18	$1a_{2u} + \text{Fe-O-S}(\sigma-\pi) \rightarrow 4e_g(\pi^*)$	
292	0.16	45	$\text{Fe-S-p/d}(\sigma) + 3e_g(\pi) \rightarrow \text{Fe}(d_z^2) + \text{O/S}(p-\sigma)$	
		24	$1a_{2u} + \text{Fe-O-S}(\sigma-\pi) \rightarrow 4e_g(\pi^*)$	
295	0.44	10	$A'(\text{Cs})(\pi) + \text{Fe-O-S}(\sigma, \pi) \rightarrow 4e_g(\pi^*)$	
		36	$\text{Fe-S-p/d}(\sigma) + 3e_g(\pi) \rightarrow \text{Fe}(d_z^2) + \text{O/S}(p-\sigma)$	
305	0.80	42	$A'(\text{Cs})(\pi) + \text{Fe}(d_{xz}, d_{yz}) \rightarrow 4e_g(\pi^*)$	
		11	$3a_{2u}(\pi) + \text{S}(px, py-\pi) \rightarrow b_{2u}(\pi^*)$	
310	0.69	18	$A'(\text{Cs})(\pi) + \text{Fe}(d_{xz}, d_{yz}) \rightarrow 4e_g(\pi^*)$	B
		44	$2a_{2u}(\pi) + \text{Fe-O-S}(p-\sigma-\pi) \rightarrow 4e_g(\pi^*)$	
312.2	0.16	40	$2a_{2u}(\pi) + \text{Fe-O-S}(p-\sigma-\pi) \rightarrow 4e_g(\pi^*)$	B
		24	$3a_{2u}(\pi) + \text{S}(px, py-\pi) \rightarrow b_{2u}(\pi^*)$	
312	0.05	29	$A'(\text{Cs})(\pi) + \text{Fe}(d_{xz}, d_{yz}) \rightarrow 4e_g(\pi^*)$	
		16	$2a_{2u}(\pi) + \text{Fe-O-S}(p-\sigma-\pi) \rightarrow 4e_g(\pi^*)$	
320	0.07	27	$a_{1u}(\pi) \rightarrow b_{2u}(\pi^*)$	
		37	$A''(\text{Cs})(\pi) + \text{Fe-O-S}(\sigma-px, py) \rightarrow \text{Fe-O1-O2}(\pi)$	
350	0.09	28	$3a_{2u}(\pi) + \text{S}(px, py-\pi) \rightarrow b_{2u}(\pi^*)$	
		22	$A''(\text{Cs})(\pi) + \text{Fe-O-S}(\sigma-px, py) \rightarrow \text{Fe-O1-O2}(\pi)$	
389	1.17	18	$A'(\text{Cs})(\pi) + \text{Fe}(d_{xz}, d_{yz}) \rightarrow 4eg(\pi^*)$	
		16	$\text{Fe-S-p/d}(\sigma) + 3e_g(\pi) \rightarrow 4eg(\pi^*)$	
394	1.05	18	$3a_{2u}(\pi) + \text{S}(px, py-\pi) \rightarrow b_{2u}(\pi^*)$	
		64	$3a_{2u}(\pi) + \text{S}(px, py-\pi) \rightarrow \text{Fe}(d_z^2) + \text{O/S}(p-\sigma)$	
414	0.04	22	$2a_{2u}(\pi) + \text{Fe-O-S}(p-\sigma-\pi) \rightarrow 4eg(\pi^*)$	B'
		28	$3a_{2u}(\pi) + \text{S}(px, py-\pi) \rightarrow 4eg(\pi^*)$	
421	0.08	34	$a_{1u}(\pi) \rightarrow 4eg(\pi^*)$	
		19	$2a_{2u}(\pi) + \text{Fe-O-S}(p-\sigma-\pi) \rightarrow 4eg(\pi^*)$	B'
471	0.24	30	$3a_{2u}(\pi) + \text{S}(px, py-\pi) \rightarrow 4eg(\pi^*)$	
		28	$a_{1u}(\pi) \rightarrow 4eg(\pi^*)$	
		20	$\text{Fe}(d_z^2/d_{xy}/d_{xz}/d_{yz}) + \text{S}(\pi) \rightarrow \text{Fe-O1-O2}(\pi)$	
		23	$A'(\text{Cs})(\pi) + \text{Fe}(d_{xz}, d_{yz}) \rightarrow d_x^2-y^2$	
		30	$3eg(\pi)/\text{Fe-O-S}(\sigma) \rightarrow \text{Fe}(d_z^2) + \text{O/S}(p-\sigma)$	
		35	$3eg(\pi)/\text{Fe-O-S}(\sigma) \rightarrow 4eg(\pi^*)$	
		44	$3eg(\pi)/\text{Fe-O-S}(\sigma) \rightarrow d_x^2-y^2$	
		71	$3eg(\pi)/\text{Fe-O-S}(\sigma) \rightarrow \text{Fe-O1-O2}(\pi)$	

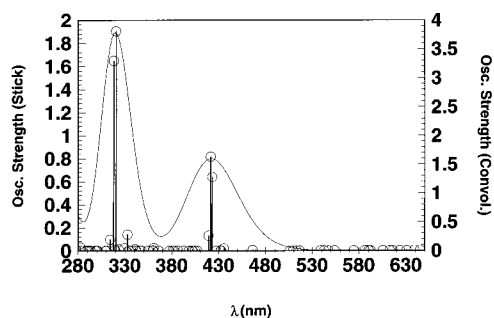


Figure 7. INDO/S/CI calculated spectrum of the reduced ferrous dioxygen porphine model P450 species at the BPW91-optimized geometry.

Table 5 gives the assignment of this spectrum in terms of the principal contributions to each of the excitation lines. As shown in Table 5, many of the excitations are from orbitals of mixed-porphyrin π and sulfur character. The origin of this dual Soret character is the mixing of sulfur p orbitals with porphyrin π and π^* orbitals that modulate the intensities of the porphyrin $\pi \rightarrow \pi^*$ excitations.

Figure 7 shows the spectrum of the reduced ferrous dioxygen porphine P450 species calculated from single excitations using the INDO/S/CI at the optimized DFT (BPW91) geometry for this species. As shown in this figure, the reduced ferrous dioxygen bound structure also has a split-Soret signature. The corresponding assignments for this spectrum in terms of fundamental excitations is given in Table 6. As shown in this table, even though the Fe–S bond elongates, sufficient S–p orbital admixture with porphyrin $\pi \rightarrow \pi^*$ orbitals occurs to account for the retention of the split Soret upon reduction.

Comparison of the Soret band positions in Figures 6 and 7 reveals that the principal consequence of the reduction of the ferrous dioxygen porphine model of cytochrome P450 is a 30-nm red shift in the Soret spectrum.

Figure 8 shows the calculated spectra of the ferrous dioxygen and reduced ferrous dioxygen protoporphyrin IX species juxtaposed with the spectrum of the high-spin camphor substrate bound protoporphyrin IX species previously reported.³¹ The calculated spectra of these three species is presented in this manner to make the closest possible comparison with the published results¹² for these three species. The experimental results are shown as an inset of Figure 8. As seen in this figure, the calculated ferric heme high-spin substrate-bound spectrum does not have a split-Soret band, while both the ferrous and reduced ferrous dioxygen species do have a pronounced split-Soret band. However, upon reduction, the lower energy component of this dual Soret band in the 400-nm region is seen to shift by about 30 nm. The spectral changes in the calculated spectra for these three species are completely analogous to the experimental results shown in the insert. The three spectra shown in this insert are for the ferric substrate bound form and two spectra reported to be associated with the ferrous dioxygen and reduced ferrous dioxygen species by Benson, Suslick, and Sligar.¹² This similarity between calculated spectra of these specific species and the observed spectra of the transient species provides independent evidence for the proposed origin of these observed spectra.

Conclusions

In this work, nonlocal DFT geometry optimizations of plausible spin states of two important dioxygen species in the

Table 6. Assignment of Major Electron Excitations Involved in the Calculated Spectral Frequencies in the Soret (B,B') Region of the Spectrum of the Reduced Ferrous Dioxygen Porphine Model P450 Species Computed from a Doublet Ground-State Reference Configuration Using INDO/S CI at the DFT Optimized Geometry

λ (nm)	osc. str.	character, %	transition character	band system
267	0.90	20.6	$2e_g(\pi) \rightarrow 4e_g(\pi^*)$	
		54.6	$3e_g(\pi) + Fe(d_{xz}, d_{yz}) + S(p_x, p_z) \rightarrow b_{2u}(\pi^*)$	
		5.8	$3a_{2u}(\pi) + S(p_z) \rightarrow 4e_g(\pi^*)$	
		4.1	$Fe(d_z^2) + O1(\sigma/\pi) + O2(\sigma/\pi) \rightarrow b_{1u}(\pi^*)$	
286	0.24	7.7	$A''(Cs) \rightarrow b_{2u}(\pi^*)$	
		40	$A'(Cs) + Fe(d_z^2) + S(p_x, p_y, p_z) \rightarrow 4e_g(\pi^*)$	
		35.5	$A''(Cs) + Fe(d_{xz}, d_{yz}) + S(p_x, p_y) \rightarrow b_{2u}(\pi^*)$	
318	0.20	45.2	$3a_{2u}(\pi) + S(p_z) \rightarrow O(\sigma)$	
		6.1	$2a_{2u}(\pi) + Fe(p_z, d_z^2) + S(p_x, p_y, p_z) \rightarrow 4e_g(\pi^*)$	
		7.9	$3e_g(\pi) + Fe(d_{xz}, d_{yz}) \rightarrow b_{2u}(\pi^*)$	
		20.3	$3a_{2u}(\pi) + S(p_z) \rightarrow 4e_g(\pi^*)$	
319	1.18	8.5	$3a_{2u}(\pi) + S(p_z) \rightarrow O(\sigma)$	
		27.2	$2a_{2u}(\pi) + Fe(p_z, d_z^2) + S(p_x, p_y, p_z) \rightarrow 4e_g(\pi^*)$	
		40.4	$3e_g(\pi) + Fe(d_{xz}, d_{yz}) \rightarrow b_{2u}(\pi^*)$	
		8.4	$3a_{2u}(\pi) + S(p_z) \rightarrow 4e_g(\pi^*)$	
323	1.33	4.1	$A''(Cs) \rightarrow b_{2u}(\pi^*)$	B
		29	$A'(Cs) + Fe(d_z^2) + S(p_x, p_y, p_z) \rightarrow 4e_g(\pi^*)$	
		11.3	$A''(Cs) + Fe(d_{xz}, d_{yz}) + S(p_x, p_y) \rightarrow b_{2u}(\pi^*)$	
		23.5	$Fe(d_z^2) + O1(\sigma/\pi) + O2(\sigma/\pi) \rightarrow 4e_g(\pi^*)$	
336	0.16	6.8	$A''(Cs) + Fe(d_{xz}, d_{yz}) + S(p_x, p_y) \rightarrow 4e_g(\pi^*)$	
		4.2	$3e_g(\pi) + Fe(d_{xz}, d_{yz}) \rightarrow b_{1u}(\pi^*)$	
		5.1	$2e_g(\pi) \rightarrow 4e_g(\pi^*)$	
		34.8	$2a_{2u}(\pi) + Fe(p_z, d_z^2) + S(p_x, p_y, p_z) \rightarrow 4e_g(\pi^*)$	
426.6	0.75	47.7	$3e_g(\pi) + Fe(d_{xz}, d_{yz}) \rightarrow b_{2u}(\pi^*)$	B'
		5.3	$1a_{1u}(\pi) \rightarrow 4e_g(\pi^*)$	
		29	$2a_{2u}(\pi) + Fe(p_z, d_z^2) + S(p_x, p_y, p_z) \rightarrow 4e_g(\pi^*)$	
		41.9	$1a_{1u}(\pi) \rightarrow 4e_g(\pi^*)$	
427	0.701	24	$3a_{2u}(\pi) + S(p_z) \rightarrow 4e_g(\pi^*)$	B'
		12.1	$A''(Cs) \rightarrow b_{2u}(\pi^*)$	
		10.3	$A'(Cs) + Fe(d_z^2) + S(p_x, p_y, p_z) \rightarrow 4e_g(\pi^*)$	
		45.3	$2e_g(\pi) + Fe(d_{xz}, d_{yz}) + S(p_x + p_y) \rightarrow b_{1u}(\pi^*)$	
		5.1	$1a_{1u}(\pi) \rightarrow b_{1u}(\pi^*)$	
		16.9	$Fe(d_z^2) + O1(\sigma/\pi) + O2(\sigma/\pi) \rightarrow 4e_g(\pi^*)$	

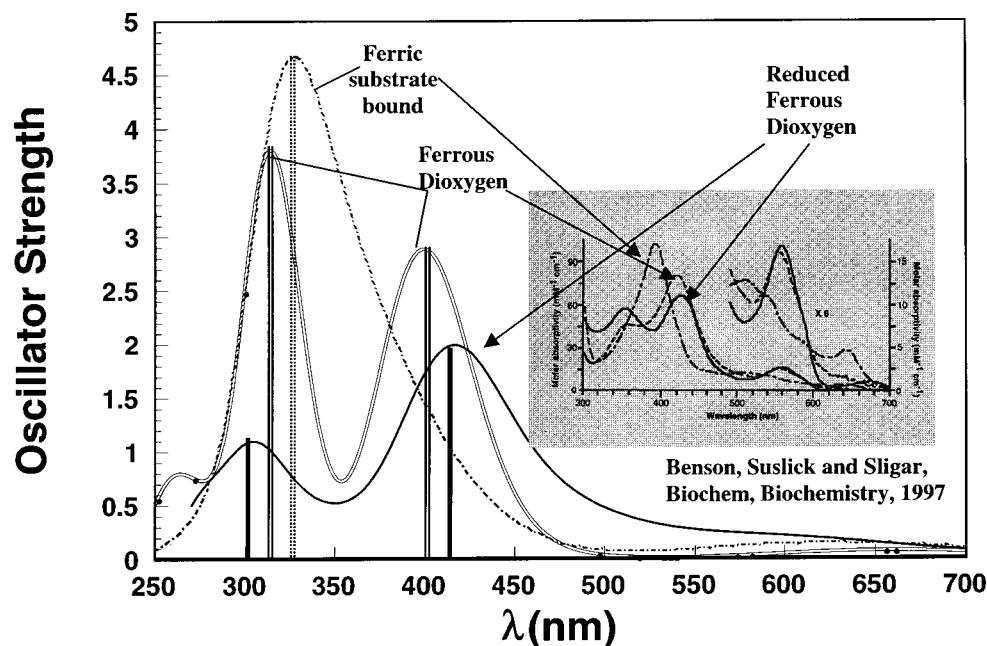


Figure 8. INDO/S/CI calculated spectra of the ferrous dioxygen and reduced ferrous dioxygen protoporphyrin-IX (heme) P450 species juxtaposed with the calculated spectrum for the ferric (high spin) substrate bound porphyrin-IX P450 species. The inset figure are the experimental spectra reported by Benson, Suslick, and Sligar, ref 12.

enzymatic cycle of P450s were performed the stable once-reduced ferrous dioxygen and the transient twice-reduced ferrous dioxygen species. The optimized ferrous dioxygen P450 heme species resulted in a structure in good agreement with the X-ray structure of a model compound for this species and with bond distances in intact proteins derived from EXAFS. The structure of the optimized ferrous dioxygen species is an asymmetric “end-on” structure with only one oxygen atom directly bound to the heme iron. Optimization of singlet and triplet species using the nonlocal DFT method resulted in a diamagnetic singlet ground state, consistent with the lack of a detectable ESR signal for this species. Calculated Mossbauer quadrupolar splitting of this singlet state is in good agreement with experimental data on cytochrome P450*cam* as well as the Weiss model compounds.

DFT optimizations of the reduced ferrous dioxygen porphine P450 species starting with an asymmetric “end-on” structure or a symmetric side-on “bridged” geometry in either a doublet or quartet spin state indicated that the “end-on” dioxygen binding mode is preferred with the alternative bridged form of this species 28 kcal/mol higher in energy. Thus, the preferred form of the reduced ferrous dioxygen species is qualitatively similar to the ferrous dioxygen species. The computed ground state from both DFT and the INDO calculations with limited configuration interaction is a doublet species. Most of the unpaired spin density is on the dioxygen ligand, consistent with the reported ESR signature of this species. Predicted Mossbauer parameters of the reduced ferrous dioxygen species doublet state are reported.

The reduction of the ferrous dioxygen porphine P450 species leads to a stable, albeit highly reactive, species. The electron adds to the lowest unoccupied molecular orbital of the ferrous dioxygen species, which has significant antibonding character in the S–Fe–O bonds. The occupancy of this orbital upon reduction results in a significant increase of the Fe–O and Fe–S bond lengths. Only minor lengthening of the O–O bond occurs as a result of the reduction. While the net negative charge on each oxygen atom increases upon reduction, a significant fraction of the added negative charge is redistributed on the

rest of the Fe–S–porphine system. Pronounced minima favorable for electropositive species in the molecular electrostatic potential (MEP) surface occur near the two oxygen atoms and the sulfur atom of the ferrous dioxygen and reduced ferrous dioxygen species. However, the depth of the electrostatic minima around the two oxygen atoms is much greater in the reduced ferrous dioxygen species. This increased negative potential minimum indicates an enhanced propensity for incipient hydrogen bonding for the reduced form. Both oxygen atoms are clearly candidates for hydrogen bonding and/or proton donation as revealed by the MEP surface.

The calculated spectra of both the ferrous and reduced ferrous dioxygen P450 heme species have a pronounced split-Soret band while the calculated high-spin substrate-bound ferric P450 heme spectrum does not. The lower energy component of this dual Soret band is shifted by ~30 nm in the reduced ferrous dioxygen species from the corresponding peak of the ferrous dioxygen species. The experimental spectra attributed to these three species exhibit similar trends in spectral shifts. This similarity between calculated spectra of specific species and observed spectra of species for which there is no independent evidence provides additional support for the hypothesized origin of the observed spectra. These combined results strengthen the assignment of these experimental spectra as originating from the ferrous dioxygen and reduced ferrous dioxygen intermediates of cytochrome P450.

Acknowledgment. The authors would like to thank Oxford Molecular for the generous access to DGauss/Unichem 4.0 in advance of release and for computer time on the Oxford Molecular J90 and gratefully acknowledge NIH grants GM 35533 (L.W.) and GM 56125 (G.H.L. and D.H.) for support.

Supporting Information Available: Two tables reporting the DFT and INDO/S absolute energies, in Hartrees, for the species considered in this work are available (1 page print/PDF). See any current masthead page for ordering information and Web access instructions.